Microscopic Origins of Shear Jamming for 2D Frictional Grains

Dong Wang, Jie Ren, Joshua A. Dijksman, Hu Zheng, and Robert P. Behringer

Phys. Rev. Lett. **120**, 208004 — Published 17 May 2018

DOI: 10.1103/PhysRevLett.120.208004

Microscopic Origins of Shear Jamming for 2D Frictional Grains

Dong Wang,[1] Jie Ren,[1,2] Joshua A. Dijksman,[1,3] Hu Zheng,[1,4,*] and Robert P. Behringer[1]

[1] *Department of Physics & Center for Non-linear and Complex Systems, Duke University, Durham, NC, USA*
[2] *Merck & Co., Inc., USA*
[3] *Physical Chemistry and Soft Matter, Wageningen University & Research, The Netherlands*
[4] *School of Earth Science and Engineering, Hohai University, Nanjing, Jiangsu, China*

(Dated: April 19, 2018)

Shear Jamming (SJ) occurs for frictional granular materials with packing fractions ϕ in $\phi_S < \phi < \phi_J^0$, when the material is subject to shear strain, γ, starting from a force-free state. Here, ϕ_J^μ is the isotropic jamming point for particles with friction coefficient μ. SJ states have mechanically stable anisotropic force networks, e.g. force chains. Here, we investigate the origins of SJ by considering small-scale structures, trimers and branches, whose response to shear leads to SJ. Trimers are any three grains where the two outer grains contacts a center one. Branches occur where three or more quasi-linear force chain segments intersect. Certain trimers respond to shear by compressing and bending; bending is a nonlinear symmetry-breaking process that can push particles in the dilation direction faster than the affine dilation. We identify these structures in physical experiments on systems of two dimensional frictional discs, and verify their role in SJ. Trimer bending and branch creation both increase Z above $Z_{iso} \simeq 3$ needed for jamming 2D frictional grains, and grow the strong force network, leading to SJ.

The transition of fluid-like to solid-like granular states, i.e. jamming, is of great theoretical and practical interest [1, 2]. Spherical grains with friction coefficient μ jam isotropically above a packing fraction, ϕ_J^μ [3, 4]. For frictional grains (discs) [5, 6] with $\phi_S < \phi < \phi_J^0$ there are unjammed, jammed, or highly anisotropic fragile states [5, 7]. According to recently reported data, $\phi_S < \phi_J^\mu$ [4, 5]. Shear jamming (SJ) in a closed system [5] and dilation in a deformable system [8] presumably share a similar origin. SJ has also been reported in suspensions [9–11], granular impacts [12] and flow [13]. Nevertheless, the origins of mechanically stable (MS) force and contact networks associated with SJ for frictional systems remain unclear. The nature of shear jamming in frictionless systems is still under investigation [14–18]. Since force networks play key roles in SJ, understanding their origins is of broad importance.

Here, we seek mechanisms for *creating* stress and MS force chains during shear, hence the origins of SJ. By contrast, shear transformation zones (STZ's), have been used extensively to model deformation and failure in amorphous molecular or frictionless systems [19–22] and have been applied to granular systems [23–25]. For frictional granular systems, buckling of force chains is the key meso-scopic failure mechanism [26]. Both STZ's and force chain buckling are failure mechanisms. However, we seek mechanisms for creating and strengthening force networks.

We propose new approaches that account for SJ: trimers (Fig. 1(c)), i.e. sequences of three particles with the center particle contacting the other two, and branches, which occur at the convergence of three or more force chain segments. We identify all trimers/branches in an experimental system and show that: 1) trimers that are roughly straight and in the compression direction,

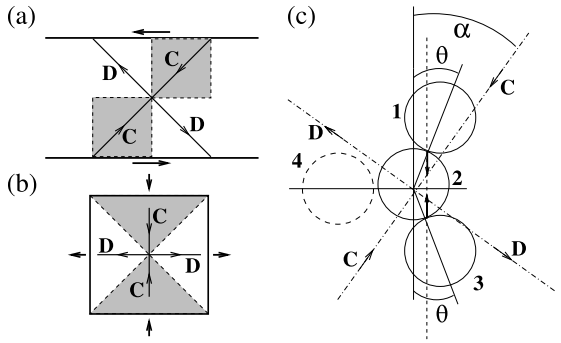

FIG. 1. (a) Sketch of simple shear with solid lines showing the principal strain directions, and neutral lines (dashed) along which there is neither compression nor dilation. (b) Sketch of pure shear showing principal directions and neutral lines similar to those of (a). In (a) and (b), the shaded regions undergo compression. (c) A sequence of three frictional grains (solid circles with numbers indicating indices) forms a trimer. θ characterizes the straightness of the trimer. α indicates the angle between the principal strain axis, and the line through the contacts between particles 1 and 2 and particles 2 and 3. In (a) – (c), C and D indicate the directions of maximum compression and dilation, respectively.

and 2) branches, play central roles in the SJ process. For any given trimer, we track as a function of shear strain, γ, its orientation relative to the compressive strain direction, α, (Fig. 1(c)), its bending angle, θ, the pressure, P, on the center particle, etc. During shear, these measures show a series of sharply defined transitions associated with the local dynamics near the trimer. To track the collective behavior of trimers, we construct a filter, O, that extracts important dynamics leading to SJ.

The experiments involved shearing a quasi-2D system of photoelastic discs, using a special simple-shear appa-

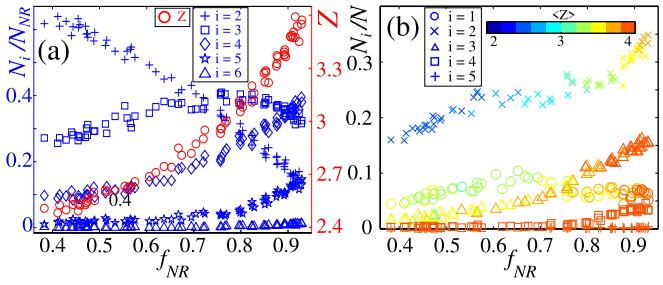

FIG. 2. (color online). Contact data vs. f_{NR} for one run with $\phi = 0.805$. (a) Blue symbols: fraction of NR particles with the indicated normalized number of contacts. Red circles: coordination number, Z. (b) N_i, the total number of particles with i strong ($f \geq \bar{f}$) contacts (and possibly other weaker contacts), normalized by N, the total number of particles in the system. The color bar gives the average Z, including moderate and weak contacts, for a given symbol.

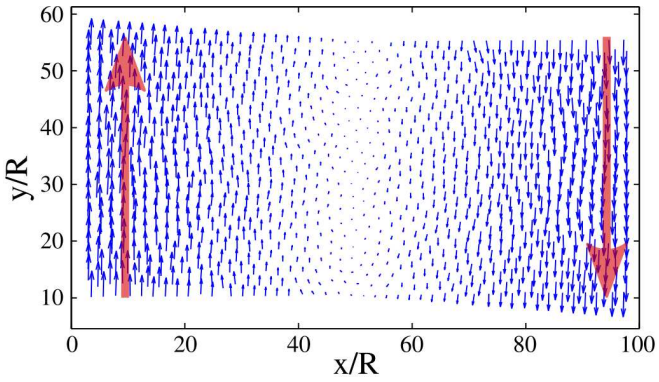

FIG. 3. (color online) Displacements (blue arrows) for each particle in units of the small particle radius, R, for $\phi = 0.805$, just at shear jamming when $\gamma = 0.0999$. Red arrows indicate the direction of simple shear.

ratus [27] with a base that deformed affinely with the boundaries, providing spatially uniform ϕ [6]. The system contained $\sim$ 1000 bi-disperse photoelastic (Vishay PSM-4) discs (friction coefficient $\mu \simeq 0.7$) of diameters 16 mm and 12.8 mm in a ratio 1 : 3.3 (large to small) whose optical properties under cross polarization yielded forces on each particle [28]. Data were obtained for five experiments for each of five ϕ's in $0.758 \leq \phi \leq 0.816$. Before each experiment, the inter-particle forces were relaxed to zero by tapping. Shear was applied in steps of $\delta\gamma = 0.0027$. After each step, we obtained images yielding positions, rotations and photoelastic responses of all particles. These data yielded contact forces, f, contact numbers on each particle, Z, and the force-moment and stress tensors. A system was deemed to be SJ if Z averaged over all non-rattler (NR) particles (those with $Z \geq 2$) was $Z \geq 3$, the minimum for mechanical stability in frictional systems [1, 2, 5].

SJ with $Z \geq 3$ occurred for all the above ϕ's, as in the representative data of Fig. 2(a) ($\phi = 0.805$) for the average Z vs. f_{NR} (red circles). f_{NR} is the fraction of NR's [5]. Z grows from $Z \simeq 2.5$, and exceeds 3. Fig. 2(a) also shows the fraction of particles, N_i/N_{NR} vs. f_{NR} for the same run. N_{NR} is the total number of NR particles and N_i is the number of particles with $Z = i$ for $i \geq 2$. Initially, the majority of NR's have $Z = 2$, but N_2/N_{NR} decreases with γ or f_{NR}, and the fractions of NR's with $Z = 3$ and $Z = 4$ grow. The data for $i \geq 3$ provide a measure of branches. Crucially, shear increases the number of particles with $Z \geq Z_{iso}$, creating a MS state. The question is: what microscale processes enable this response?

Also important is the relation between a particle's contact number and the mean force it experiences. Here, we consider two groups, based on the particle's contact forces, f, relative to the system-wide mean, $\bar{f}$, at a given γ. 'Strong' force particles have at least one $f \geq \bar{f}$. 'Weak' force particles have all $f < \bar{f}$. A similar thresholding was validated by k-core percolation analysis [5].

We now restrict N_i to the total number of particles with i *strong contacts* (and possibly other weaker contacts), normalized by N, the total number of particles in the system. These are the 'force chain' particles. Fig. 2(b) shows data for these N_i/N, where color gives the mean Z; e.g., crosses give the number fraction of particles with exactly two strong contacts, and possibly other weaker contacts. Initially, the $N_i = 2$ particles have Z close to 2, but as f_{NR} increases, Z reaches $Z \sim 3$ near $f_{NR} \simeq 0.7$. This means that initially, quasi-linear force chains (with strong binary contacts) dominate the strong network. But, as shear progresses the strong force network particles gain contacts, modifying the network structure as force chains emerge in the dilation direction [5]. This is a hallmark of SJ.

During shear, particles follow trajectories that are close to affine, as shown in Fig. 3. Hence, understanding changes in the contact network, requires measures that are sensitive to the small departures from affine motion. We need: 1) a basic building block that accounts for local bending/curvature of force chains, and 2) an accounting of branches. A minimal structure for 1) is captured by trimers, exemplified by three consecutive particles in a force chain. Force chains consist of a series of partially overlapping trimers. More generally, a trimer, Fig. 1(c), is three particles (e.g. 1, 2, 3), where the central particle contacts the other two. Branches occur where three or more force chain segments converge, e.g., particles with three or more contacts as in Fig. 4(c). The number of branches reflects the random structure of packings, the improbability of finding long stable chains with only two contacts per particle, and the shear-induced growth of contacts, in particular by trimer bending.

We consider the response to shear of a trimer that is part of, or becomes part of, a force chain. Shear consists of compression and dilation in orthogonal directions, e.g.

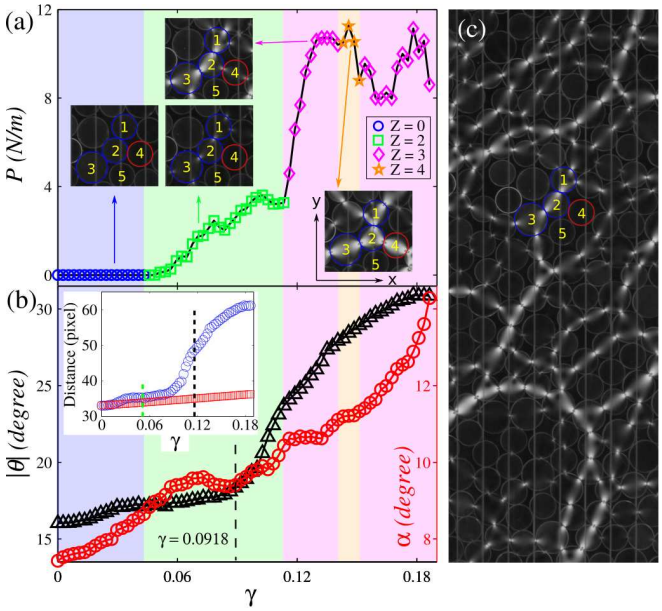

FIG. 4. (color online). Representative example of trimer response to shear. (a) P for particle 2 and photoelastic images of the trimer (particles 1-2-3) vs. γ. Z for particle 2 is indicated by different symbols. At $\gamma = 0.1161$, 2 contacts 4, and P on 2 starts to rise quickly. When $Z = 4$, 2 makes weak contact with 5. In the lab frame (inset) the coordinates are x-y, with shear along y. The compression direction is along $\sim 45°$. (b) Opening angle, θ (black triangles), and orientation α (red circles) of the trimer. (b)-inset: distance from particle 2 to the line connecting the centers of 1 and 3 (blue circles) and the corresponding distance if every particle moved affinely with the shear (red squares). (c) A broader region around the trimer of (a) for $\gamma = 0.108$.

Fig. 1(a)-(b). Intuitively, trimer response to shear depends on the angle α relative to the compression direction (Fig. 1(c)). For small α, compression pushes particles 1 and 3 toward 2, closing contacts/increasing contact forces on 2. This may also bend the trimer, increasing θ. For trimers aligned in the dilation direction (large α), shear tends not to directly act on the trimer (assuming non-cohesive particles); rather, such a trimer may exhibit nonaffine motion due to collisions with neighboring particles.

Since particles move close to their affine trajectories, how does shear increase Z and P, and enable the force network in the dilation direction? Roughly straight trimers with small α bend under shear, and in so doing, push the central particle (particle 2, Fig. 1(c)) in the dilation direction faster than the rate of affine dilation (see proof in [27] that bending of a trimer with $\alpha = 0$ after a shear strain of γ pushes the center particle by a distance $\Delta = \cot^2\theta(1+\gamma)^{-1}$ times that induced by the affine dilation; $\Delta > 1$ for most relevant θ's. See example in Fig. 4(b)-inset discussed below). That is, compression-induced bending pushes 2 toward 4 faster than 4 could move away under affine dilation. This leads to 1) an additional contact on 2 from 4, 2) a new branch point, 3) the formation of force networks in the dilation direction, and 4) SJ and/or dilatancy, with only moderate relative motion of particles. In experiments, bending is routine for trimers that are roughly in the compression direction. Unlike STZ's, trimer bending in force chains corresponds to local displacements that break the symmetry about the y-axis: particles 1 and 3 move symmetrically about the x-axis. But generally, there is no mirror image particle for 2 due to the low probability of adjacent force chains.

To demonstrate the importance of trimers in an experiment, we first show that under shear, a single typical trimer lying in the compression cone, $|\alpha| < \pi/4$, undergoes complex dynamics, including bending and contact formation. We then present a measure, O, that captures the collective evolution of trimers.

Fig. 4 tracks the geometric and force response of a trimer in the compression direction. We label the particles 1, 2 and 3 in the insets of Fig. 4(a), which show photoelastic images of the region around this trimer. A broader region is shown in Fig. 4(c) and [27]. At first, Fig. 4(b), the trimer bends slowly with γ, i.e. $|\theta|$ increases, and α rotates somewhat faster than the affine strain. Initially, there is no force on particle 2, but at $\gamma \simeq 0.051$, P on particle 2 shows a sharp transition, and grows roughly linearly with γ due to compressive strain pushing 1 and 3 against 2. At $\gamma = 0.0918$, θ shows a sharp transition. The trimer bends much more rapidly with γ, creating a contact between 2 and 4 when $\gamma = 0.1161$, hence a branch. This initially weak contact is along the dilation direction, and associated with a second transition in the P vs. γ data for 2. Eventually, more complex behavior occurs; P on particle 2, α, and θ all grow. By $\gamma = 0.18$, $\theta \simeq 30°$, has nearly doubled, indicating substantial bending. The force network in the dilation direction associated with 4 has grown significantly. Fig. 4(b)-inset shows the distance from particle 2 to the line connecting the centers of particles 1 and 3 (blue circles), vs. the same distance if every particle moved affinely with the applied shear strain (red squares). Clearly trimer bending pushes the center particle faster than the affine strain.

The above example typifies trimer bending, creation of new contacts, and the emergence of the network in the dilation direction. Here we define a measure, O, to capture the key geometric trimer properties θ and α. A simple though not unique measure with both properties of a trimer is $O = -[(\hat{b}_i \cdot \hat{b}_j - c_{ij})/[A(1+c_{ij})] \cdot cos(2\alpha)]$, where $\hat{b}_i$ and $\hat{b}_j$ are unit vectors from the origin of the central particle (e.g. 2 in Fig. 1(c)) to the two other trimer particles (e.g. 1 and 3), and c_{ij} is the maximum value of $\hat{b}_i \cdot \hat{b}_j$ (when 1 and 3 touch). $\cos(2\alpha)$ is > 0 (< 0) for the compression (dilation) cone. O will decrease if a trimer in the compression direction bends or if one in the

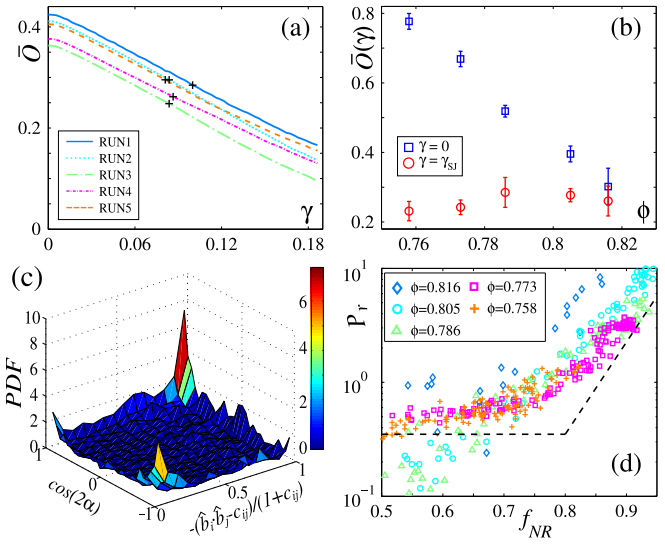

FIG. 5. (color online). (a) $\bar{O}$, for trimers in the force network at SJ for five runs with $\phi = 0.805$, with the black crosses indicating when Z just reaches 3. (b) $\bar{O}$ values averaged over five runs for each density, blue squares: $\gamma = 0$; red squares: γ_{SJ}. (c) Two dimensional PDF of O vs. $-(\hat{b}_i \cdot \hat{b}_j - c_{ij})/(1 + c_{ij})$ and $\cos(2\alpha)$ for run 1 in (a) when Z just reaches 3. (d) Rescaled pressure P_r for the trimers with $O \geq 0$ vs. f_{NR}, for five ϕ's. Black dashed line: fit for P_r for trimers with $O < 0$ (see SM for more details [27]).

dilation direction straightens. If θ and α for a collection of trimers are uniformly distributed, the mean value of O for the compression (dilation) cone would be 0.378 (-0.378) for the normalization constant $A = 1$. Henceforth, we choose $A = 0.378$, so that a uniform distribution of trimers in the compression cone is unit normalized.

To characterize global trimer evolution, we first compute the average, $\bar{O}$, of a special set (SS) of trimers that form the force network in an experiment at the onset of SJ, $Z = 3$. This collectively describes dynamics of the most important trimers that might otherwise appear as random motion. Fig. 5(a) shows $\bar{O}$ vs. γ for five runs at $\phi = 0.805$, for which SJ occurs at $\gamma_{SJ} \simeq 0.1$. $\bar{O}$ starts at a positive value because trimers in the SS, i.e. in the strong network at jamming, are often roughly straight trimers aligned in the compression region. $\bar{O}$ decreases nearly linearly with γ, supporting the expectation that, statistically, force chains in the compression cone bend under shear. $\bar{O}$ at $\gamma = 0$ varies from run to run due to different initial conditions, but the slope $d\bar{O}/d\gamma$ is nearly the same for each run.

Fig. 5(b) compares $\bar{O}$ at $\gamma = 0$, and at SJ, for which $\gamma = \gamma_{SJ}$. Given that the data of Fig. 5 correspond to only the fraction of trimers that become part of the force network at jamming, the initial values of $\bar{O}$ are significant. $\bar{O}(\gamma_{SJ})$ is less than $\bar{O}(0)$, and is nearly independent of ϕ, indicating a common/universal $\bar{O}$ at SJ. The nonzero value of $\bar{O}(\gamma_{SJ})$ indicates an anisotropic network when the system reaches a shear jammed state. The fact that $\bar{O}(0)$ increases as ϕ decreases towards ϕ_S, the lower limit for SJ, indicates that the force network at jamming draws increasingly from trimers that tend to be straighter and more compression-aligned.

We note that trimers in the dilation cone with moderate θ have negative values of O, and tend to straighten under shear. But for $\gamma < \gamma_{SJ}$, these trimers typically do not experience large forces unless one of the particles is also part of a trimer that is oriented in the compression cone (or until the system has become jammed).

More details on the individual contributions of the θ and α components of O are given in Fig. 5(c). This shows the 2D probability function (PDF) of O for the SS at shear jamming as a function of $-(\hat{b}_i \cdot \hat{b}_j - c_{ij})/(1 + c_{ij})$ (x-axis) and $\cos(2\alpha)$ (y axis). There are two peaks; the largest by far is near $(x, y) \sim (1, 1)$; a smaller one is near $(0, -1)$. The smaller corresponds to largely bent trimers in the dilation direction. The larger corresponds to fairly straight trimers in the compression direction, i.e. to much of the strong force network.

We next examine the correlation between the geometric evolution of trimers and stresses by computing P_r, the pressure for trimers, rescaled by P at jamming. Fig. 5(d) shows P_r vs. f_{NR} for particles belonging to all trimers with $O \geq 0$. Data for different ϕ tend to collapse at and above $f_{NR} \approx 0.7$, indicating universal behavior. The dashed lines show the contribution from the remainder of the particles; for clarity, these data are represented by fits to results shown in Fig. S3 of the SM [27]. P_r for $O \geq 0$ dominates and begins to rise at a much lower f_{NR} than P_r for the $O < 0$ trimers. Thus, $O \geq 0$ trimers, distinguished by their geometry, form the backbone of force networks in the shear jammed state.

In summary, we propose novel structures and mechanisms enabling shear jamming for frictional discs: 1) particular trimers, roughly straight triplets of particles aligned in the compression direction, can strengthen and bend under shear, pushing particles in the dilation direction faster than the affine dilation; and 2) branches, which connect force chain segments. Trimer bending is an intrinsic part of SJ. It helps generate the transverse network, increasing Z and the number of branches. Trimers with moderate α typically respond to increasing γ with increasing local pressure, bending, and rotation. O identifies collective geometric trimer properties, and is correlated with the particles carrying the majority of the forces/pressure. Branches provide a second mechanism for generating stable structures and for raising Z above Z_{iso}. Initially, force chain branches are present because the probability of long nearly straight force chains is low. But bending increases Z and the number of branches.

Trimer bending and branch formation are not unique to shear. They presumably occur during other types of strain. Since the resulting force networks, particularly for SJ, are not isotropic, bulk response functions must

reflect this anisotropy. Force networks and microscopic structures in three dimensions present a future challenge, where generalized trimer bending may be relevant. The mechanism of trimer bending considered here for frictional particles may apply for frictionless particles. For $\mu = 0$, if bending occurs, larger bending angles would be needed to reach the 2D $Z_{iso} = 4$ for frictionless particles, in comparison to $Z_{iso} = 3$ for 2D frictional ones.

Discussions with Bulbul Chakraborty and Stefan Luding are gratefully appreciated. This work was supported by NSF grants DMR-1206351 and DMS-1248071, NASA grant NNX15AD38G, the William M. Keck Foundation, DARPA, and a Triangle MRSEC fellowship for DW. HZ thanks NSFC Grant No. 41672256 for financial support.

* hz64@phy.duke.edu

[1] M. van Hecke, J. Phys.: Condens. Matter **22**, 033101 (2010).
[2] B. Chakraborty and R. P. Behringer, in *Encyclopedia of Complexity and Systems Science*, edited by R. Meyers (Springer, New York, 2009) pp. 4997–5021.
[3] C. S. O'Hern, L. E. Silbert, A. J. Liu, and S. R. Nagel, Phys. Rev. E **68**, 011306 (2003).
[4] L. E. Silbert, Soft Matter **6**, 2918 (2010).
[5] D. Bi, J. Zhang, B. Chakraborty, and R. P. Behringer, Nature **480**, 355 (2011).
[6] J. Ren, J. A. Dijksman, and R. P. Behringer, Phys. Rev. Lett. **110**, 018302 (2013).
[7] M. E. Cates, J. P. Wittmer, J. P. Bouchaud, and P. Claudin, Phys. Rev. Lett. **81**, 1841 (1998).
[8] O. Reynolds, Phil. Mag. **20**, 469 (1885).
[9] R. Seto, R. Mari, J. F. Morris, and M. M. Denn, Phys. Rev. Lett. **111**, 218301 (2013).
[10] I. R. Peters, S. Majumdar, and H. M. Jaeger, Nature **532**, 214 (2016).
[11] A. Fall, F. Bertrand, D. Hautemayou, C. Mezière, P. Moucheront, A. Lemaître, and G. Ovarlez, Phys. Rev. Lett. **114**, 098301 (2015).
[12] A. H. Clark, A. J. Petersen, L. Kondic, and R. P. Behringer, Phys. Rev. Lett. **114**, 144502 (2015).
[13] M. Grob, C. Heussinger, and A. Zippelius, Phys. Rev. E **89**, 050201 (2014).
[14] H. A. Vinutha and S. Sastry, Nature Physics **12**, 578 (2016).
[15] N. Kumar and S. Luding, Granular Matter **18**, 58 (2016).
[16] M. Baiti-Jesi, C. P. Goodrich, A. J. Liu, S. R. Nagel, and J. P. Sethna, J. Stat. Phys. **167**, 735 (2016).
[17] E. Azéma, F. Radjai, and J. N. Roux, Phys. Rev. E **91**, 010202(R) (2015).
[18] O. Imole, N. Kumar, V. Magnanimo, and S. Luding, KONA Powder and Particle Journal **30**, 84 (2013).
[19] M. L. Falk and J. S. Langer, Phys. Rev. E **57**, 7192 (1998).
[20] D. Pan, A. Inoue, T. Sakurai, and M. W. Chen, Proc. Natl. Acad. Sci. **105**, 14769 (2008).
[21] C. A. Schuh and A. C. Lund, Nature Materials **2**, 449 (2003).
[22] K. W. Desmond and E. R. Weeks, Phys. Rev. Lett. **115**, 098302 (2015).
[23] W. Li, J. M. Rieser, A. J. Liu, D. J. Durian, and J. Li, Phys. Rev. E **91**, 062212 (2015).
[24] G. Lois, A. Lemaître, and J. M. Carlson, Phys. Rev. E **72**, 051303 (2005).
[25] A. Le Bouil, A. Amon, S. McNamara, and J. Crassous, Phys. Rev. Lett. **112**, 246001 (2014).
[26] A. Tordesillas, J. Zhang, and R. P. Behringer, Geomechanics and Geoengineering **4**, 3 (2009).
[27] See Supplemental Material for a detailed description of the experimental setup, the proof showing that bending of trimers with small α pushes the central particle faster than the affine dilation, a broader region showing particles response, and pressure for particles below the O threshold.
[28] T. S. Majmudar and R. P. Behringer, Nature **435**, 1079 (2005).